

Optic disc segmentation using a matching filter and a deformable model

C.MARIÑO, N.BARREIRA, M.G.PENEDO, M.HORTAS, A. PÉREZ-URRÍA, J.L.DONCEL, F.GONZÁLEZ[†]
 Grupo de Visión Artificial y Reconocimiento de Patrones

University of A Coruña
 Campus de Elviña s/n, A Coruña, 15071

[†]University of Santiago de Compostela

[†]School of Medicine and Complejo Hospitalario Universitario of Santiago, 15782 Santiago de Compostela
 SPAIN

Abstract: This paper presents an algorithm for automatic extraction of the optic disc in retinal digital images. The developed system consists of two main parts. Firstly, a clustering algorithm is used to select the regions which contain the pixels with the highest gray levels. A correlation filter is applied to these regions to compute the approximate center of the optic disc. Then, in order to extract the optic disc, a deformable model which works in three stages is used. The localization of the region of interest is successful in 98.5% of the cases and the optic disc is correctly extracted in 93% of the cases.

Key-Words: Matching filter, segmentation, optic disc, deformable model.

1 Introduction

The retinal fundus photographs are widely used in the diagnosis of eye diseases. Processing automatically a large number of retinal images can help ophthalmologists to increase the efficiency in medical environment.

The optic disc is the brightest area in images that have not large areas of exudates and it is a slightly oval disc. It is the entrance region of vessels and its detection is very important since it works as a landmark for the other features in the retinal image.

There are many previous works on optic disc localization. Lalonde et al. [1] extract the optic disc using Hausdorff-based template matching and pyramidal decomposition. It is neither sufficiently sensitive nor specific enough for clinical application.

On the other hand, strategies based on active contours [2-4] are used to detect the optic disc boundary in retinal images. These techniques are very robust against noise but their main disadvantage is their high computational cost.

In this paper, a methodology to extract the optic disc is proposed. Firstly, a clustering algorithm is used to compute the regions with highest gray level pixels. A correlation filter is applied to these regions in order to compute the approximate center of the optic disc. Once the optic disc position is located, a deformable model is used to obtain an accurate segmentation of its

boundary. This last stage follows the work of Lowell et al. [3], but with our own implementation.

The chosen deformable model is composed by a global model and a local model. The global model fits approximately to the boundary of the optic disc. The local deformable model can get a more accurate fit to the characteristics of the boundary, keeping at the time the shape of the model when the boundary does not exist or it is difficult to get. Optic disc segmentation is performed in three stages: in the first two stages the global model is fitted to the optic disc. In the third stage, starting from the result of the previous stages, the local model is accurately fitted to the particularities of the boundary of the optic disc.

This work is organized as follows: first section introduces the problem and several approaches which can be found in literature to solve the problem of optic disc segmentation. Second section describes the optic disc localization algorithm, which allows to find the precise location of the optic disc head. Third section describes the segmentation algorithm, showing the three stages the deformable model used in the segmentation step performs in. Fourth section shows the results obtained by the combination of both previous algorithms, and finally in last section conclusions and future work are discussed.

2 Optic disc localization

The first stage of the process consists of locating the region where the optic disc is located. A clustering algorithm is used to compute the regions with highest gray level pixels, among which will be the one containing the optic disc. Later, a correlation filter is applied to these regions in order to discard the regions where the optic disc is not located, and to compute the approximate center of the optic disc in the right region. With the addition of the clustering algorithm to the whole process proposed by Lowell et al. a better performance has been obtained, improving results by reducing the wrong localization cases, as will be shown in results chapter.

2.1 A clustering algorithm

Since the intensity of the optic disc is much higher than the retinal background, a possible method in order to localize the optic disc is to find the largest clusters of pixels with the highest gray levels. For this reason, the pixels with the highest 1% gray levels are selected. After this, a clustering algorithm groups the nearby pixels into clusters. Initially, each point is a cluster and its own centroid. If the Euclidean distance between two centroids is less than a specified threshold ϵ , these clusters are combined to form a new one. The new centroid (c_x, c_y) is computed by means of Equations 1 and 2.

$$c_x = \sum_{i=0}^n \frac{x_i}{n} \quad (1)$$

$$c_y = \sum_{i=0}^n \frac{y_i}{n} \quad (2)$$

where (x_i, y_i) are the cluster points and n is the number of points in the cluster.

If there are bright areas as well as the optic disc in the retinal image, the algorithm might compute several clusters. The regions of interest are defined as $n \times m$ rectangles whose centers are the centroids of these clusters. The rectangle size depends on the image resolution.

Figure 1 shows the points which the clustering algorithm is applied to. It is also depicted the regions of interest computed by means of this process.

2.2 Correlation filter

As depicted in Figure 1(f), several regions of interest might be computed by means of the clustering algorithm because of bright areas in the retinal images. A correlation filter is applied to each region in order to locate the true region where the optic disc is situated.

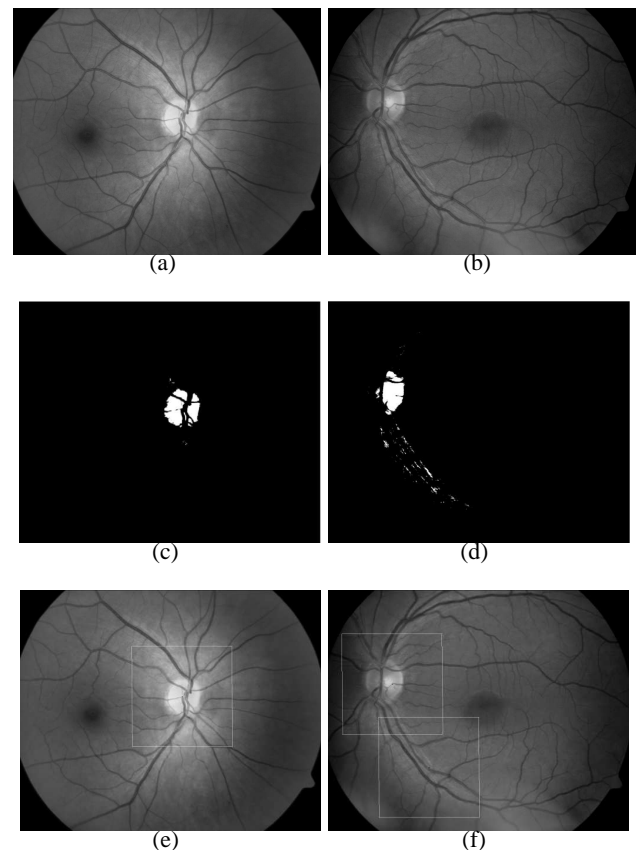


Fig 1: Top: original digital retinal images. Middle: selected points (highest 1% gray levels) which the clustering algorithm is applied to. Bottom: the regions of interest computed by means of the clustering algorithm when applied to images 1(a) and 1(b).

The optic disc consists of a high intensity near-circular disc, with a roughly centrally band of low intensity vessels. Due to this fact, the template consists of a Laplacian of Gaussian with a vertical channel in the middle to correspond to the major vessel band. This correlation filter is shown in Figure 2.

The template is correlated with the intensity component of the retinal image. We use the full Pearson-R correlation to take variations in mean, intensity and contrast into account, as defined in Equation 3.

$$C_{i,j} = \frac{\sum_{x,y} (f(x,y) - \bar{f}(x,y))(w(x-i,y-j) - \bar{w})}{\sqrt{\sum_{x,y} (f(x,y) - \bar{f}(x,y))^2 \sum_{x,y} (w(x-i,y-j) - \bar{w})^2}} \quad (3)$$

where \bar{w} is the mean value of the template and \bar{f} is the mean value of the area covered by w .

The region of interest containing the optic disc is defined as $n \times m$ rectangle whose center is the point with the higher response computed by means of the correlation filter. Figure 3 shows the final region of interest of a retinal image in which the clustering algorithm computed two different regions.

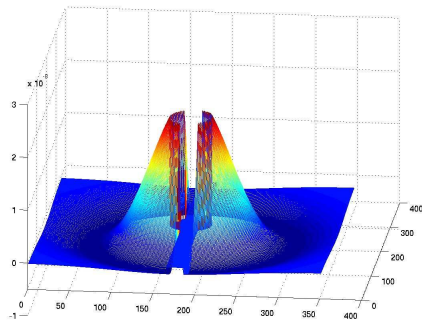


Fig 2: The correlation filter, where the template consists of a Laplacian of Gaussian with a vertical channel in the middle corresponding to the major vessel band

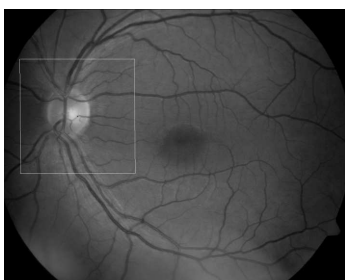


Fig 3: Region of interest defined as $n \times m$ rectangle whose center is the point with the higher response computed by the correlation filter applied to the regions shown in Figure 1(f), showing only the right region where the optic disc is located in, and discarding the wrong region.

3 Optic disc segmentation

Once the region containing the optic disc is computed, the extraction of the optic disc is performed by means of a deformable model.

Deformable models or snakes were introduced by Kass et al. [5], and since then they have widely studied and many different models have appeared [6–8] among others, resulting in an invaluable tool for the medical images analysis [7, 9–11]. In this work the deformable model used in the segmentation performs like the proposed by Hu et al. [12], but with some improvements to get a better segmentation of the optic disc nerve head.

Firstly, will briefly introduce Hu’s work, in order to explain later the improvements applied to this first proposal.

3.1 Hu’s circular model

The deformable model from Hu et al. [12] works by combining two models: a global model and a local model. The global model is a circle with center \mathbf{c} and radius r , and is used to get a rough fitting to the border of the optic disc. The local model is defined by the center \mathbf{c} and evenly spaced radial spokes, and direction vector $s_i = [\cos(\theta_i), \sin(\theta_i)]$. The model is defined by distances m_i from \mathbf{c} along each spoke. The local model has a corresponding global model with radius $r = \bar{m}_i$, the local model’s mean radial displacement.

The force f which guides the process has two components: an internal force f^{int} and an external force f^{ext} . The forces work along the radial spokes. The external force drags the model toward the attractor points. The internal force limits model deformation using two components: global force, which pulls the model toward the global shape, and the local force, which smoothes the model by penalizing differences in deformation between neighboring spokes.

3.2 Alterations to the Hu’s circular model

Three modifications were introduced in the Hu’s model, following the work from Lowell et al. [3]:

1. **A global elliptic model**, to get a better fit to the elliptic shape of the optic disc.
2. **Use of the vector gradient**, to detect changes in the radial spokes’ intensity, and finally,
3. **use of energy functions** to support fast nonlinear optimization.

3.2.1 The global elliptic model

The global model is an ellipse with a vertical principal axis and a fixed aspect ratio a (Figure 4).

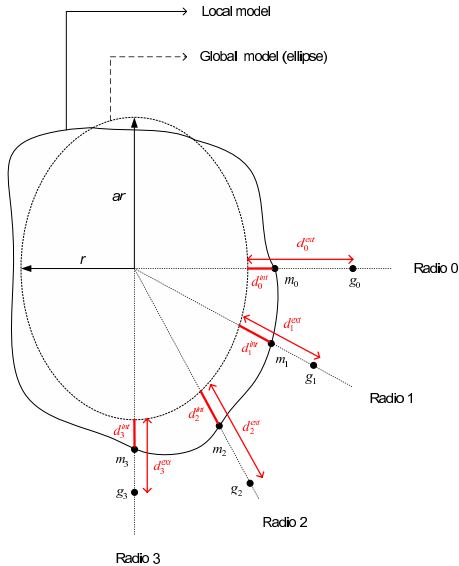


Fig 4: Global elliptic model and local deformable model.

Global model has a corresponding local model with radius defined by equation 4.

$$r = \frac{1}{S} \sum_i \frac{m_i}{a_i} \quad (4)$$

3.2.2 Gradient vector

In Hu's work, negative gradient magnitude was used to compute the forces. Here the smoothed normalized gradient vector image Υ (see eq. 5) is used.

$$\Upsilon = \nabla I / \max(\|\nabla I\|) \quad (5)$$

Points which attract the model can be chosen using the directional information from the gradient vector. Points from the border of the optic disc will have a gradient vector direction pointing outside the optic disc, in a radial direction. This way, attractor points should have the same gradient direction than the radial vector direction of the spoke they are located over. So, the final gradient magnitude in a point with distance ρ from \mathbf{c} along the spoke i is defined by equation 6.

$$\gamma_i(\rho) = \left(\sum_{xy} w_{x,y} \Upsilon(x,y) \right) \cdot \mathbf{s}_i \quad (6)$$

where $w_{x,y}$ is defined by equation 7 (see Figure 5)

$$x_d = |p_x - x| \quad y_d = |p_y - y|$$

$$w_{x,y} \begin{cases} (1 - x_d)(1 - y_d) & (x_d < 1) \wedge (y_d < 1) \\ 0 & \text{otherwise} \end{cases} \quad (7)$$

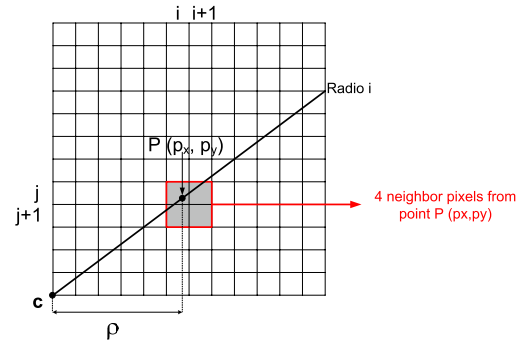


Fig 5: Scheme of the bilinear interpolation used to compute the magnitude of the gradient vector in the attractor points.

3.2.3 Energy functions

A fast nonlinear optimization procedure is performed to minimize the deformable model energy function, the Quasi-Newton [13]. This method requires explicit energy functions and a gradient function.

Energy functions are defined as the sum-squared of the model's deformation from the attractors, as shown in equation 8.

$$E^{xy} = \frac{1}{2} \left\| \left(\frac{1}{S} \sum_i m_i^n - c \right) \right\|^2 \quad (8)$$

where

$$E = E^{ext} + E^{int} = E^{ext} + E^{glo} + E^{loc} \quad (9)$$

where external energy (E^{ext}), energy of the global model (E^{glo}) and energy of the local model (E^{loc}) are defined as

$$E^{ext} = \frac{1}{2} \sum_i (g_i^n - m_i^n)^2 \quad (10)$$

$$E^{glo} = \frac{1}{2} \sum_i \beta_i (m_i^n - r)^2 \quad (11)$$

$$E^{loc} = \frac{1}{2} \sum_i \beta_i \alpha (m_i^n - \langle m_i^n \rangle)^2 \quad (12)$$

Differentiating E^{xy} with respect to \mathbf{c} and E with respect to m_i^n , we get the required gradient functions, shown in equations 13 to 17.

$$\frac{dE^{xy}}{dc} = \frac{1}{S} \sum_i m_i^n \mathbf{s}_i \quad (13)$$

$$\frac{dE}{dm_i^n} = \frac{dE^{ext}}{dm_i^n} + \frac{dE^{glo}}{dm_i^n} + \frac{dE^{loc}}{dm_i^n} \quad (14)$$

$$\frac{dE^{ext}}{dm_i^n} = g_i^n - m_i^n \quad (15)$$

$$\frac{dE^{glo}}{dm_i^n} = \beta_i \left((m_i^n - \overline{m_i^n}) - \overline{(m_i^n - \overline{m_i^n})} \right) \quad (16)$$

$$\frac{dE^{loc}}{dm_i^n} = \beta_i \alpha [(m_i^n - \langle m_i^n \rangle) - \langle (m_i^n - \langle m_i^n \rangle)] \quad (17)$$

To choose the parameters, the same approaches than the chosen in [3] were implemented.

3.3 Segmentation algorithm

Finally, whole the segmentation process is described in this section.

Once the optic disc rim is located by means of the localization algorithm described in the second section, the first stage of the segmentation process is performed, adjusting the global model to the temporal border of the optic disc. Then, the second stage fits approximately the global model to the whole optic disc rim. Finally, third stage fits the local model to the optic disc border, getting a much more precise segmentation.

4 Results

To test the accuracy of the localization and segmentation algorithms described below, a set of 135 images were used as the benchmark. Images were acquired in different centers of the Complejo Hospitalario Universitario de Santiago de Compostela (CHUS), all of them with a Cannon CR6-45NM Non-Mydriatic Retinal Camera, with a 768×576 pixel resolution. Although the camera originally captures color images, a conversion to gray-level images (with 256 gray levels) was performed prior to the application of the algorithms, since color does not provide any useful information.

Validation of the algorithms was performed by expert clinicians of the CHUS, who analyzed the output of the techniques to set its accuracy.

Images in the test set presented a high variability in features like optic disc shape and diameter, summarized in Table 1.

To validate our experiments, two expert clinicians segmented manually the optic nerve head from the test

	Horizontal diameter	Vertical diameter	Rate (a)
Mean	158.281	169.430	1.071
Std.deviation	12.739	12.591	0.056
Maximum	220	225	1.207
Minimum	130	146	0.942

Table 1: Some statistic of the measures of optic discs, obtained from images in the test set, showing the high variability among them. First column shows the horizontal diameter, second column vertical diameter, third column the rate between them. The values correspond to the mean, standard deviation, maximum value and minimum value from the measures (in pixels) taken in the images of the test set.

images, and these results were compared with the results obtained by the application of the process described in the preceding sections. Result from that comparisons is shown in Table 2, where three categories were defined (good, fair, poor), function of the difference between the results obtained by clinicians and automatic results. This discrepancy for image j was computed using equation 18.

$$\delta^i = \sum_i \frac{|m_i^j - \mu_i^j|}{\sigma_i^j + \varepsilon} \quad (18)$$

with μ_i^j and σ_i^j summarizing the clinician's choice of rim location on spoke i of image j , and $\varepsilon = 0.5$ a small factor to prevent division by zero.

	Localization		
	Good	Fair	Poor
Number images	85	48	2
%	62.963	35.556	1.481
	98.519 %		1.481 %
	Segmentation		
	Good	Fair	Poor
Number images	44	82	9
%	32.592	60.741	6.667
	93.333 %		6.667%

Table 2: Results obtained in each stage (localization and segmentation) of the process. Three quantitative categories were defined (good, fair, poor), with disparities one, two or more, respectively, computed using equation 18

Analyzing results shown in Table 2, both the stages of the algorithm, localization and segmentation, give an mean effectiveness of 95.5%, which is superior to that of Lowell et al., where algorithm was first proposed.

To illustrate these results, Figure 6 depicts several result images from the localization (first column) and segmentation (second column) stages, and with good (a-b), fair (c-d) and poor (e-f) results.

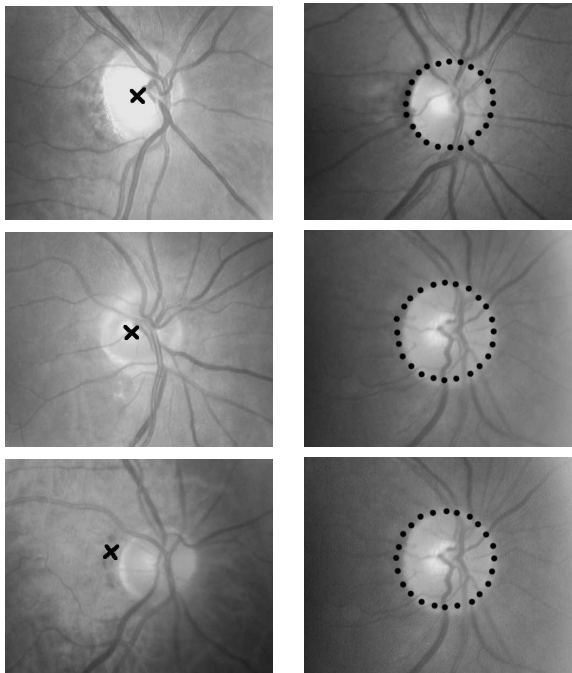


Fig 6: Result images from the localization (left column) and segmentation (right column) stages, with the three different categories of results: good (top row), fair (middle row) and poor (bottom row) results.

5 Conclusions and future work

In this work an algorithm for the precise localization and segmentation of the optic disc nerve head has been presented. The algorithm performs in two stages: in the first, the region of interest where the optic disc is located is obtained by combining a clustering process with a posterior correlation procedure. The size of the central channel (corresponding to the main optic disc vessel) has been estimated, with a mean size in the test set of 20 pixels, which is also the size of this area in the correlation kernel. By other side, the size of this filter has been calculated for the set of images in the test set, getting sizes from 130px to 220px. Since the filter must have at least the size of the bigger optic disc, commented results have been obtained with a kernel of 221×221 px, which have performed well for the whole set of images. Results from this first stage show a successful percentage of 98.519%, with only 2 errors in 135 cases, improving the results from Lowell et al.

In the second stage, the located optic disc is segmented through a deformable model, proposed by Lowell et al. and which we re-implemented with very good results (successful percentage of 93.3%). In order to set the parameter values for the segmentation models, mean horizontal radio for the optic disc was computed in the images of the test, giving a result of 80px, value which was taken as the ellipse horizontal

initial radius value. The second parameter to tune, the a ratio, was also set by taking the mean value in the images of the test set, and finally the value in the experiments was set to 1.06, giving very good results, as shown above. In the Hu's equations, α was set to the value proposed in their work: $\alpha = 0.5$. Finally, radial search length value m_i was set to 8 in the first stage of the segmentation process, 6 in the second stage and 4 in the third, more accurate fitting stage.

The whole process has taken an average time of 1.4 seconds in the experiment performed, with a set of 135 different digital retinal images.

In the future work we will test the algorithm with a wider set of images, trying to evaluate the effect of images with diseases like diabetic retinopathy in the results. By other side, we are working in a technique which will allow for the segmentation of the whole retinal vascular tree, together with the optic disc, which will serve for the improvement in the evaluation of the patients with eye-diseases.

Acknowledgements: This paper has been partly funded by the Xunta de Galicia through the grant contracts PGIDT04PXIC10501PN and PGIDT03TIC10503PR.

References

- [1] Lalonde M., Beaulieu M., and Gagnon L. Fast and robust optic disk detection using pyramidal decomposition and Hausdorff-based template matching. *IEEE Transaction on Medical Imaging*, vol. 20, 2001, pp. 1193–1200.
- [2] Mendels F., C. H., and J.P. T. Identification of the optic disk boundary in retinal images using active contours. *Proceedings of the Irish Machine Vision and Image Processing Conference*, 1999, pp. 103–115.
- [3] Lowell J., Hunter A., Steel D., Basu A., Ryder R., Fletcher E., and Kennedy L. Optic nerve head segmentation. *IEEE Transactions on medical Imaging*, vol. 23, 2004, pp. 256–264.
- [4] Chanwimluang T. and Fan G. An efficient algorithm for extraction of anatomical structures in retinal images. *IEEE International Conference on Image Processing*, vol. 23, 2004, pp. 1093–1096.
- [5] Kass M., Witkin A., and Terzopoulos D. Active Contour Models. *International Journal of Computer Vision*, vol. 1(2), 1988, pp. 321–331.
- [6] Bro-Nielsen M. Active Nets and Cubes, 1994.

- [7] Cootes T.F., A. Hill C.J.T., and Haslam J. Use of active shape models for locating structures in medical images. *Image and Vision Computing*, vol. 12(6), 1994, pp. 355–365.
- [8] Giraldi G., Strauss E., and Oliveira A. Dual-T-Snakes model for medical imaging segmentation. vol. 24(7), 2003, pp. 993–1003.
- [9] Pardo X.M., Carreira M.J., Mosquera A., and Cabello D. A snake for CT image segmentation integrating region and edge information. *Image and Vision Computing*, vol. 19(7), 2001, pp. 461–475.
- [10] Hang X., Greenberg N.L., and Thomas J.D. A geometric deformable model for echocardiographic image segmentation. *Computers in Cardiology*, (4), 2002, pp. 77–80.
- [11] Yan P. and Kassim A.A. Medical image segmentation with minimal path deformable models. vol. 4, 2004.
- [12] Hu Y.L., Rogers W.L., Coast D.A., Kramer C.M., and Reicheck N. Vessel boundary extraction based on a global and local deformable physical model with variable stiffness. *Magnetic Resonance Imaging*, vol. 16, 1998, pp. 943–951.
- [13] Press W., Teukolsky S., Vetterling W., and Flannery B. *Numerical Recipes in C*. 2nd ed. Cambridge University Press, 1992.